Published by IOP Publishing for Sissa Medialab

Received: *March 19, 2019*
Revised: *August 30, 2019*
Accepted: *September 6, 2019*
Published: *September 30, 2019*

Nonlocal thresholds for improving the spatial resolution of pixel detectors

B. Nachman[a,b] **and A.F. Spies**[c,1]

[a] *Physics Division, Lawrence Berkeley National Laboratory, Berkeley, CA 94704, U.S.A.*
[b] *Simons Institute for the Theory of Computing, University of California, Berkeley, Berkeley, CA 94720, U.S.A.*
[c] *Department of Physics, University of California, Berkeley, Berkeley, CA 94720, U.S.A.*

E-mail: alex@afspies.com

Abstract: Pixel detectors only record signals above a tuned threshold in order to suppress noise. As sensors become thinner, pitches decrease, and radiation damage reduces the collected charge, it is increasingly desirable to lower thresholds. By making the observation that hit pixels tend to be spatially close to each other, we discuss two schemes for dynamic threshold adjustment which could be realized at the level of frontend electronics: one utilizing cross-talk originating from capacitive coupling between neighboring pixels, and the other requiring the use of a nominal high threshold and a triggerable low neighbor threshold. These schemes are tested in the context of single particle simulations with a single pixel layer following the specifications of upcoming ATLAS and CMS detector upgrades. By adjusting the parameters of each algorithm, we find that the pixel cluster position resolution in both schemes is more stable under threshold changes than the default fixed threshold approach. These dynamic threshold methods may have important implications for pixel readout chip design at the Large Hadron Collider and other future colliders.

Keywords: Detector modelling and simulations II (electric fields, charge transport, multiplication and induction, pulse formation, electron emission, etc); Electronic detector readout concepts (solid-state); Particle tracking detectors; Solid state detectors

[1]Corresponding author.

https://doi.org/10.1088/1748-0221/14/09/P09028

2019 JINST 14 P09028

Contents

2019 JINST 14 P09028

1 Introduction

Pixel detectors are designed to be thin, to be highly granular, and to have low occupancy in order to precisely reconstruct charged-particle trajectories (tracks) from minimum ionizing particles (MIPs).[1] In order to achieve this goal while maintaining a high signal efficiency, only signals above a tuned threshold are recorded. This threshold is chosen to be small compared to a typical signal, but large compared to noise. For example, sensors in the current LHC experiments ATLAS and CMS are 200–300 µm thick, leading to a signal at perpendicular incidence of 16k-24k electrons (e); noise levels (measured as the equivalent noise charge or ENC) are typically 100–150e and tuned thresholds are 2k-3ke. With these settings, the noise occupancy is well below 10^{-6} [1, 2].

Given the increased instantaneous luminosity at the HL-LHC and the goal of improving track reconstruction, there is a move towards thinner and narrower sensors. Such sensors will require lower thresholds to compensate for the reduced signal charge resulting from the decreased path length of MIPs. At the same time, the high particle flux expected at the HL-LHC also poses challenges as increased radiation damage will lead to progressive decline in collected charge over the lifespan of pixel sensors whilst also increasing the noise due to the sensor leakage current [3]. The ATLAS and CMS collaborations are working together within the RD53 collaboration [4] to develop a new readout chip for their HL-LHC pixel detectors and therefore now[2] is a critical time

[1] While not all measured charged particles are at the exact minimum of the ionization curve, this is the commonly used term to refer to particles with $\beta\gamma \gtrsim 1$.

[2] Given that both ATLAS and CMS are designing their innermost layers to be replaceable, new ideas may still see utilization in subsequent years, even if they are not fully developed in time for the upcoming production runs.

to find solutions that address, at least in part, the challenges associated with the next-generation of pixel designs. To this end, we propose two dynamic methods for pixel thresholding which stem from a simple, but significant observation about MIP and noise hits: while the probability for a single pixel to be hit by a MIP is 0.1% or smaller [5, 6], the probability for a pixel to fire (above a fixed threshold) given that one of its neighboring pixels was hit is 10% or more [7]. While the neighboring pixel hits can be caused by charge sharing from diffusion and capacitive coupling, they can also be due to an inclined primary particle traversing multiple sensors at an angle. Coupled with the fact that noise hits exhibit no spatial correlation, this suggests that the optimal threshold should depend on the pattern of neighboring hits.

The first proposed method is to intentionally share some fixed fraction of deposited charge between neighboring pixels by taking advantage of capacitive coupling between the frontend electronics. While this form of charge sharing has been well-studied in the literature (see e.g. ref. [8]), it is traditionally viewed as a nuisance. Secondly, we propose the implementation of two distinct fixed thresholds in the frontend, such that if a pixel goes above threshold its neighbors switch to a reduced threshold.

We are not aware of any previous efforts to utilize neighboring pixel information to dynamically adjust thresholds via frontend electronics. There have been previous proposals to implement dynamic thresholds to correct for spatial-temporal effects using information from a particular pixel [9]. A related topic is dual thresholds, which have been used extensively to separate time and energy measurements in order to make the best of both for a single detection. This technique has been applied to precision timing ($\mathcal{O}(10\,\text{ps})$) applications as diverse as positron emission tomography detectors [10] and high energy physics timing detectors [11–14] as well as 'standard' LHC pixel detectors with time-walk concerns at $\mathcal{O}(10\,\text{ns})$ timescales [15]. Dual thresholds have also been used for improving the position resolution by using one threshold for event triggering and one for measuring charge in regions of interest [16]. Futhermore, commercial ALiBaVa devices provide three distinct triggers which can be adjusted at the firmware level, allowing for enhanced cluster detection in microstrip detectors [17]. Such schemes are complementary to our proposals, which implement multiple thresholds in the front-end electronics directly.

This paper is organized as follows: section 2 outlines the simulation setup and evaluation methods used, and section 3 details the proposed threshold schemes. Results are presented in section 4 with a brief discussion on implementation in section 5; the paper ends with conclusions and outlook in section 6.

2 Methodology

2.1 Simulation

A standalone simulation setup using Allpix [18] built on the Geant4 package [19] is used to simulate single particles interacting with a single planar pixel layer. The sensor specifications are similar to those proposed for the ATLAS and CMS pixel detector upgrades for the HL-LHC [5, 6]. In particular, the sensors are 150 µm thick with a pitch of $50 \times 50\,\mu\text{m}^2$. The simulation of energy deposition, drift, and digitization is the same as in ref. [20] and is briefly summarized here for completeness.

2019 JINST 14 P09028

Charge deposition and straggling are provided by Geant4 using the EMSTANDARD_OPT0 model.[3] The ionization energy is converted into electron-hole pairs assuming 3.6 eV/pair and electrons are transported to the collecting electrode, including drift and diffusion. Collected electrons are digitized using a Time over Threshold (ToT) method [22], with a linear charge-to-ToT conversion.[4] The analog threshold is varied, but the number of bits is fixed at four, as suggested in ref. [20] and shown to have little impact on the resolution. Unless otherwise specified, the sensors are modeled without radiation damage. The effects of radiation damage are approximated by reducing the collected charge according to the n^+-in-n planar sensor results based on combining TCAD simulations from the Perugia [23] and New Delhi models [24] with drift, diffusion, and digitization presented in ref. [5].

2.2 Performance metrics

Three important rates that are tied to the choice of threshold are the signal efficiency, the occupancy,[5] and the noise rate. The signal efficiency is the fraction of collected charge from a MIP; this is not always one, as charge that diffuses to a neighboring pixel or is at the outskirts of a cluster may be below the threshold. The threshold can also be used to control the overall hit rate in order to ensure that the occupancy is manageable. For pixel detectors at the HL-LHC, the occupancy will be dominated by real hits and not noise. However, the total occupancy still has a large contribution due to non-MIP hits. Since it is difficult to accurately model the low-energy spectrum, instead of providing the total occupancy, we report the contribution of MIPs to the occupancy. Finally, as the noise rate is well below the overall occupancy, it is important to report the error rate separately.

One of the important consequences of a reduced charge collection efficiency with increased threshold is that the estimated position resolution worsens. Alongside the quantities utilized for evaluation described above, we also report the position resolution as a function of the threshold setting.[6] The resolution provides a measure of the deviation between reconstructed and true particle incidence positions, with the reconstruction based on statistical correlations between the structure of over-threshold pixels for a given event (a set of such over-threshold pixels being referred to as a *cluster*). For a cluster of length L_{cluster}, as shown in the bottom of figure 1, all of the information about the position in the y (long) direction as well as the longitudinal incidence angle is contained in y_{head}, which is the location of the particle as it traversed the first pixel in the cluster. As the tail and head position resolutions are approximately the same, the resolution on the position estimator $y_{\text{cluster}} = \frac{1}{2}(y_{\text{head}} + y_{\text{tail}})$ is $\sigma_{y_{\text{head}}}/\sqrt{2}$, while the resolution on the cluster length $y_{\text{head}} - y_{\text{tail}}$ is $\sqrt{2}\sigma_{y_{\text{head}}}$. Since the deposited charge scales with path length, one can use the amount of deposited charge in the first pixel to estimate the location y_{head}.

In order to produce reconstructed position estimates from deposited charge and y_{head}, we define the estimator $\hat{y}_{\text{head}}(Q) = \mathbb{E}[y|Q]$ which minimizes the mean squared error, where Q is the

[3] This is not accurate for thin sensors, but 200 µm are sufficiently thick that the total deposited charge is well-modeled [21].

[4] ToT is used by ATLAS and RD53A, but the exact details of the digitization method are not critical for the results presented here, which apply a linear scaling between charge and the digital value.

[5] In this work we use occupancy as a measure of fractional pixel activation. This includes counting how many pixels have charge deposited during MIP traversal, and determining whether the charge deposited pushes a pixel above the threshold.

[6] Non-linear charge interpolation for position estimation is a well-established practice (see e.g. ref. [25]). The optimal construction is briefly reviewed here to elucidate the subsequent analysis and discussion.

2019 JINST 14 P09028

(digitized) charge deposited in the first pixel (i.e. the "head" of the cluster). Explicitly, we calculate the position resolution as $\sqrt{\langle(\hat{y}_{\text{head}} - \langle\hat{y}_{\text{head}}\rangle)^2\rangle}$ and note that this quantity is approximately bounded by pitch$/\sqrt{12}$ [26]. The top right plot in figure 1 shows the distribution of traversed distance through the first pixel in a cluster against the first pixel's charge, at a threshold of 600e. As expected, the charge of the first pixel increases linearly with traversed distance, up to the point where the MIP has passed through the entire sensor. However, due to significant straggling, this correlation is not exact.

The true value of y is defined to be zero at the start of the pixel and all resolutions are normalized by the pitch. The left side of figure 1 illustrates three scenarios in which the value of $\hat{y}_{\text{head}}$ can vary, and the corresponding regions are delineated by horizontal lines on the histogram to the right. Notably, in rare circumstances, enough charge can diffuse to a pixel adjacent to the first traversed pixel, to result in a cluster with negative $\hat{y}_{\text{head}}$. In addition, the threshold can be sufficiently high that the first traversed pixel is below threshold, resulting in values of $\hat{y}_{\text{head}}$ greater than 1. Each of these cases are illustrated schematically in the left diagrams of figure 1. Pixels due to δ-rays are excluded from the analysis as they register an anomalously high charge that has little to do with the position of the original MIP. Especially for δ-rays that travel many pixels before reaching their Bragg peak, the non-MIP signature can be identified and removed before estimating the MIP position. The occurrence of δ-rays for the first pixel in a cluster is about 1%.

3 Threshold schemes

We consider three schemes for setting charge thresholds:

- **Nominal.** If the charge is below the threshold, then the ToT is zero. This is the usual way a fixed threshold is implemented: a comparator takes the output of the pixel pre-amplifier and compares it with a fixed threshold.

- **$f_{\text{share}} = X\%$.** Pixel modules already exhibit a form of dynamic thresholds due to capacitive coupling between adjacent pixels (often called referred to as 'cross-talk'), stemming from inductive effects whose complete mitigation would require preamplifiers with infinitely large feedback capacitances; such cross-talk leads to effective charge sharing between neighboring pixels.[7] This provides one implementation of the proposed *charge sharing* scheme whereby when a charge q is deposited in one pixel, the neighboring pixels register $f_{\text{share}}q$, resulting in an effective decrease in the threshold of pixels adjacent to a hit pixel by an amount $f_{\text{share}}q$. It is worth noting that cross-talk effects scale in proportion to the length of shared edges, and that in practice the value of f_{share} is typically specified to be as small as possible, often about a few percent [8]. We propose to engineer f_{share} so as to optimize the occupancy and resolution. In practice, designing a pixel with a given f_{share} while also simultaneously meeting other specifications may prove difficult, however, our goal is to study the impact of a larger f_{share} in order to motivate future studies in a real chip. It is worth noting that we assume square pixels, and thus add $f_{\text{share}}q$ to the four neighbors sharing an edge and subtract $4f_{\text{share}}q$ from the primary pixel. Additionally, for all other schemes, f_{share} is set to zero. This mechanism that shares charge also shares noise — this is ignored in the results below, which is justified by appendix B.

[7] An introduction to the physics of these effects may be found in §3.2.1 of ref. [8].

2019 JINST 14 P09028

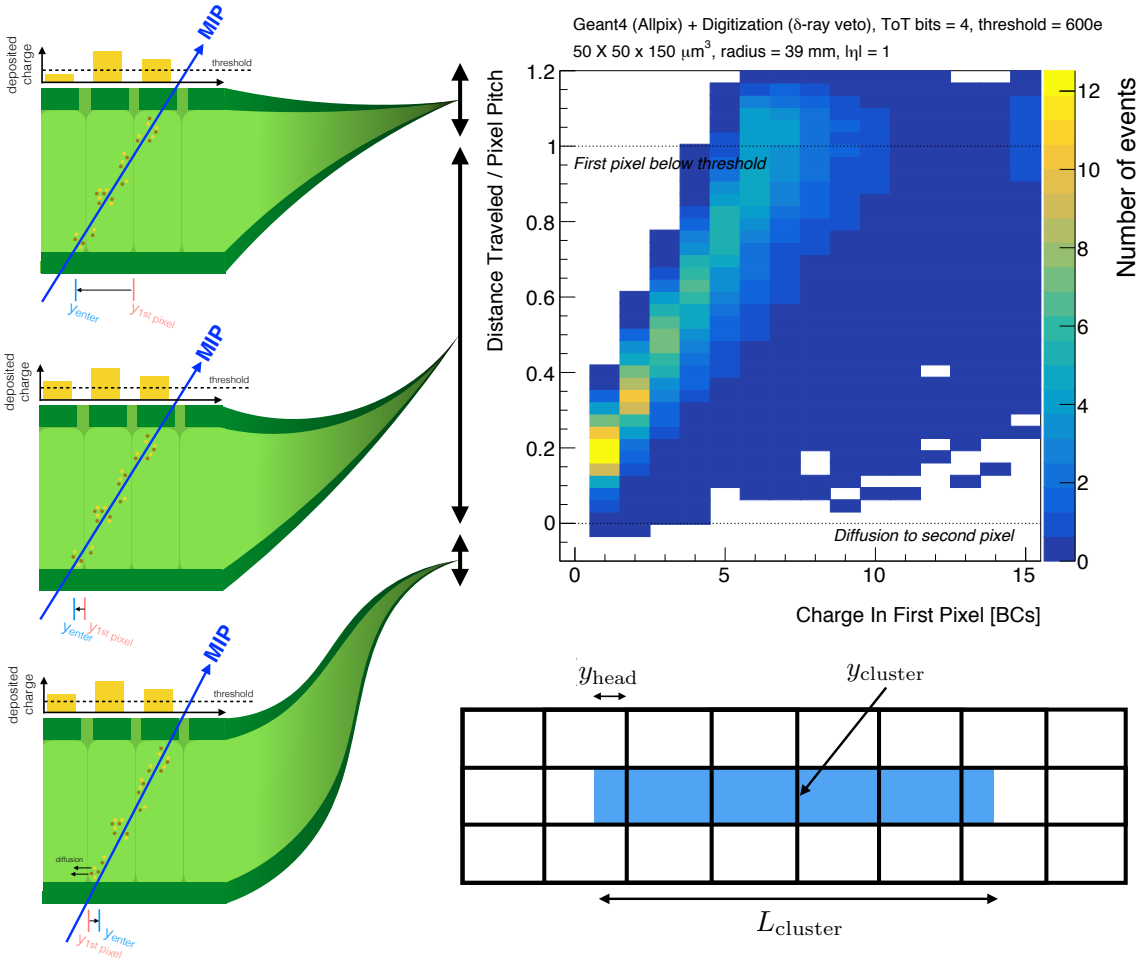

Figure 1. A schematic diagram to illustrate the calculation of the effective position resolution. The bottom right figure shows a pixel cluster, where the filled regions indicate the path of a MIP. All of the information about the position and length of the cluster are contained in y_{head} and y_{tail}; since the resolution of these two quantities should be approximately the same, we focus only on the former quantity. The top right plot shows the distribution of the position traversed by a MIP normalized per bin of measured charge. The left figures illustrate the definition of $\hat{y}$, which can be negative if enough charges diffusion into the previous pixel and can be more than 1 if the first traversed pixel is below threshold.

- $f_{\mathrm{neighbor}} = X\%$. Charge sharing provides an indirect method for dynamic thresholds; instead, we propose to directly set the threshold of a given pixel based on the activity in neighboring pixels. The simplest such scheme is to have two thresholds: a nominal high threshold and a lower threshold equal to f_{neighbor} of the high one. Then, if a pixel goes above the high threshold, all of its neighbors see a lower threshold. In practice, this would require explicit information sharing between pixels and may require significant added capacitance and/or power. However, section 4 will show that this is a powerful scheme for maintaining both high efficiency and good position resolution.

Before presenting results, we note that the latter two schemes affect only a fractionally small number of pixels for any given event, and therefore have a negligible impact on the overall noise rate.

2019 JINST 14 P09028

4 Results

Figure 2 shows the MIP efficiency and charge efficiency for first traversed pixel in a cluster, as well as the MIP efficiency measured over all pixels, as a function of the threshold for the three schemes introduced in section 3. In the case where the efficiencies are only given for the first traversed pixel in the cluster, the MIP charge efficiency is much higher than the efficiency to register any hit; this is a consequence of the fact that the charge in the first pixel is small when the path length is short. As expected, increasing the threshold degrades both the (charge) efficiency. For the chosen values of $f_{\text{share}} = 5\%$ and $f_{\text{neighbor}} = 50\%$, the hit efficiency is improved for every threshold. The f_{neighbor} scheme also has a higher MIP charge efficiency than the nominal approach.

Additionally, the f_{share} approach appears to have a lower MIP charge efficiency than the nominal approach, but this is an artifact caused by the increased charge from the neighbor as after digitization, it cannot be distinguished from the primary charge. Notably, the MIP efficiency is 5–10% higher with the new threshold schemes. The plot on the right of figure 2 essentially shows the average fractional amount of pixels which go over threshold in a given scheme. As expected, this shows the same trend, but with the cross-talk scheme causing an increased rate of hit-losses relative to the other schemes (an effect which manifests most significantly on the edges of clusters, and is thus supressed in the plot on the left).

For reference, the left plot of figure 2 also shows the noise rate, assuming ideal Gaussian noise, in which the rate decreases exponentially with increasing threshold. In practice, the noise is not exactly Gaussian, and the suppression with increased threshold is not as strong as indicated. However, the fact that the noise rate is still significantly suppressed with increasing threshold, coupled with the trends shown in figure 2, indicate that it is possible to have a higher threshold without compromising the MIP (charge) efficiency.

Figure 3 contains two plots: the first illustrating the variation of position resolution with threshold in the three schemes under investigation, and the second showing the resolution as a function of f_{share}.

Focusing first on the left plot, we see that the two new schemes improve the resolution for all values of threshold, and that the resolution worsens with increasing threshold, akin to the MIP efficiency. Furthermore, with a value of $f_{\text{neighbor}} = 50\%$, the triangle points in the left plot are the same as the nominal points with a threshold reduced by 50%. The improvement from the $f_{\text{share}} = 5\%$ scheme is more modest, but is still a few percent for all thresholds. Additionally, the shallow trend of the direct-talk scheme implies that increased thresholds could be applied with relatively less detriment to the resolution than in the other two schemes.

The right plot highlights the sensitivity of the resolution to the exact amount of cross-talk. Interestingly, there is an optimal amount of charge sharing at 5% for the given incidence angle, pitch, threshold, and charge tuning. This is to be expected, as increasing f_{share} from zero improves the resolution until information about the charge from the first pixel is washed out by the contribution from the neighbor that went over the threshold. The absolute change in the resolution is about 2%, but subtracting in quadrature, the additional resolution is about 20%.

The intense radiation environment of current and future hadron colliders is one of the greatest challenges for silicon-based pixel detectors. Figure 4 shows the position resolution as a function of the non-ionizing energy loss for a fixed threshold. Since charge is lost from charge trapping, the

2019 JINST 14 P09028

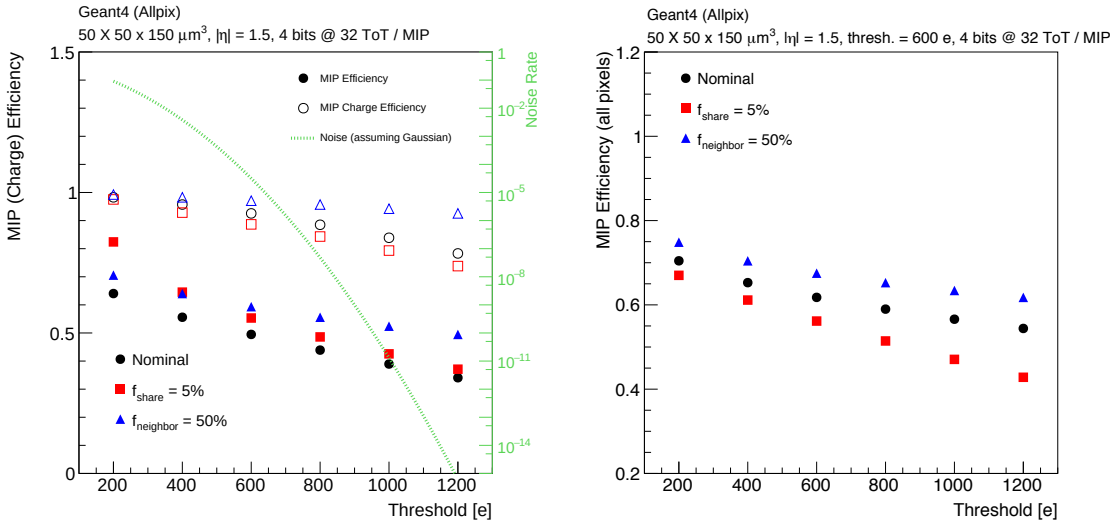

Figure 2. Left: the MIP (charge) efficiency as a function of the threshold for the three threshold schemes; for reference, the noise rate is also given assuming an ideal 150e Gaussian noise profile. Right: the MIPs Efficiency measured over all pixels in which charge was deposited or shared. In both cases, MIPs are incident a slight angle (corresponding to $\eta = 1.5$) in order to increase the pixel multiplicity in clusters along the longitudinal direction. The ToT is tuned so that a MIP at perpendicular incidence would correspond to a ToT of 32 if 15 were not the maximum value.

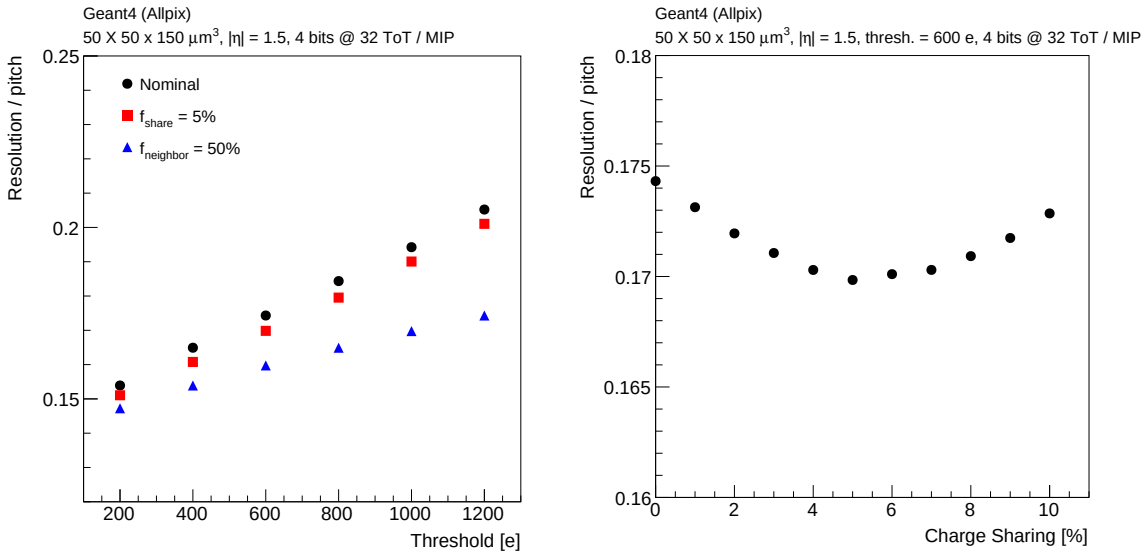

Figure 3. Left: the y_{head} position resolution as a function of the threshold for the three schemes. Right: the y_{head} position resolution as a function of the charge sharing (f_{share}). In both cases MIPs are incident at $\eta = 1.5$, with the same charge tuning as in figure 2.

2019 JINST 14 P09028

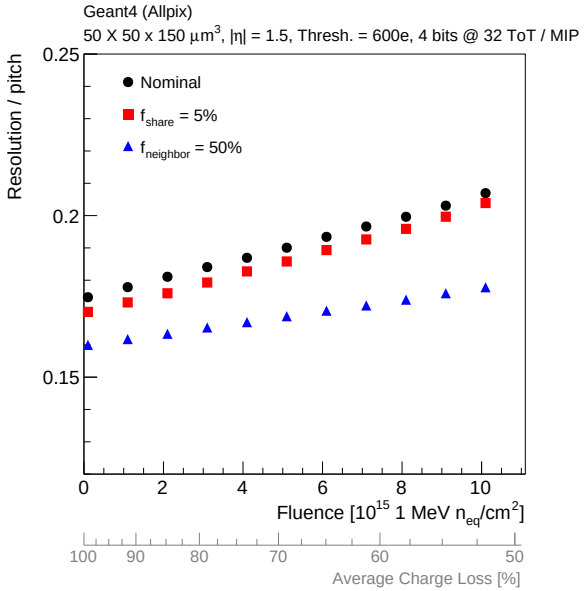

Figure 4. The position resolution as a function of the silicon 1 MeV $n_{\mathrm{eq}}/\mathrm{cm}^2$ fluence for the three threshold schemes at a fixed threshold of 600e and with the same tuning as figure 2. The average charge loss from ref. [5] is given as a second axis.

resolution degrades with fluence. The innermost layers of the HL-LHC detectors will need to cope with about 10^{16} 1 MeV $n_{\mathrm{eq}}/\mathrm{cm}^2$. Given the assumptions going into figure 4, the $f_{\mathrm{neighbor}} = 50\%$ scheme has the same position resolution after the full HL-LHC fluence as the nominal scheme does with an unirradiated sensor. The clear superiority of the direct scheme with respect to radiation hardness is unsurprising as it is the least severely affected by changes in signal-size which are not significant enough to drive pixels under threshold.

5 Discussion

Using capacitive coupling to implement the dynamic threshold has the advantage that the information from the primary hit is transferred nearly instantly to the neighboring pixels. The disadvantage is that designing a specific amount of capacitive coupling is challenging, especially given the tight constraints from other design requirements (including noise and power consumption).

In the alternative scheme where active logic is used to reduce the threshold on the neighbors, information must be quickly sent to the neighboring pixels. Figure 5 illustrates this time constraint when one hit passes the initial high threshold and a neighboring hit would only pass a reduced threshold. The first clock cycle where this hit is recorded to be above the high threshold is t_0 and the first clock cycle for which the smaller hit would be above the reduced threshold is t_1, while it goes below this threshold at t_2. This second hit will be recorded as long as the second threshold can be reduced in a time $t_2 - t_0$. The charge resolution of the second hit will be optimal when the communication time is only $t_1 - t_0$; any will result in a degraded resolution. This fast communication must fit within a stringent timing and power budget for the readout design.

2019 JINST 14 P09028

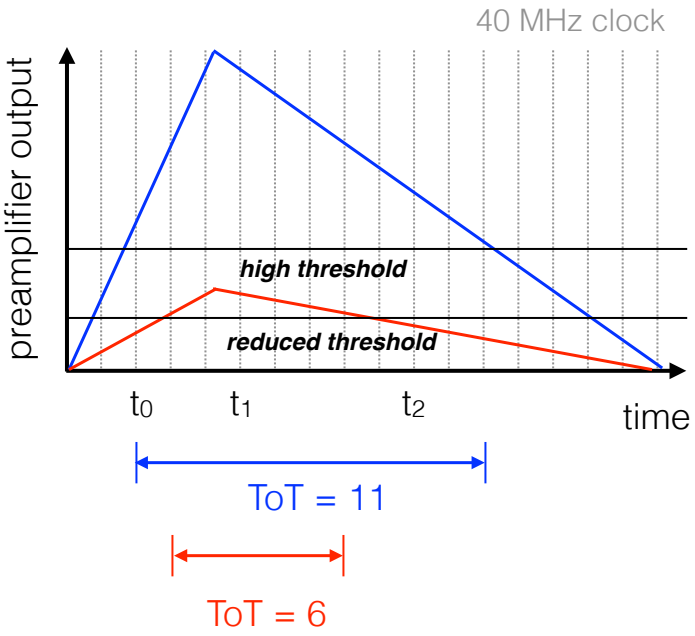

Figure 5. A schematic illustration of the charge digitization for two particles: one with a large charge (blue) and one with a small charge (red); the fact that the blue charge goes over threshold faster is known as 'time-walk'. The small charge particle does not pass the initial high threshold, but would pass the reduced threshold if the new threshold could be set before t_2. The ToT for the small charge in this scheme would be at most 6, when the threshold is reduced by t_1.

It is also worth noting that the potential use of asymmetric pixels at the LHC has been studied, as these allow the preferential trade-off in position resolution along longitudinal or transverse directions. While all results presented in the previous section were carried out on symmetric pixels, in appendix A we present approximate results for scheme-dependent resolution variation as a function of pixel asymmetry.

6 Conclusions

The HL-LHC presents significant challenges for pixel module design and now is the time to consider new possibilities for optimizing the information saved for offline analysis. We have presented two schemes for dynamic thresholds which use information from neighboring pixels in order to increase the MIP efficiency, with little or no increase in the noise rate. One scheme exploits the unavoidable interpixel capacitance to effectively share charge between neighboring pixels, yielding a lower effective threshold. Notably, we found that, from the perspective of position resolution, there is an optimal amount of charge sharing. While in practice it may be difficult to engineer a particular level of charge sharing, given other specifications, these results suggest that design studies are worthwhile, especially in light of the challenges posed by the HL-LHC conditions. However, one drawback of this scheme is that the effective decrease in the threshold is statistically distributed and varies significantly with the straggling of MIP charge depositions.

2019 JINST 14 P09028

Secondly, we propose a scheme which instead utilizes two fixed thresholds, thus circumventing the aforementioned challenge. This algorithmically simple scheme presents a lower threshold to all pixels adjacent to a pixel which exceeds a high, nominal threshold. This procedure significantly improves the resolution and MIP efficiency, but practical implementations would depend on a mechanism for rapid communication between neighboring pixels. Indeed, adding circuitry for this purpose would certainly increase the capacitance and/or the power consumption; the consequences of which require further investigation in order to weigh the benefits of this scheme in practical implementations.

Signal efficiency and position resolution are crucial for both track reconstruction and flavor tagging at the LHC, and thus it is conceivable that the trade-offs of the proposed dynamic threshold schemes may be outweighed by the gains. Certainly, considerable amounts of potentially useful information are present in the neighborhood around pixels which are not being explicitly used, and which could significantly improve detector performance for the HL-LHC and beyond.

Acknowledgments

We would like to thank Maurice Garcia-Sciveres and Timon Heim for many useful discussions as well as the RD53 collaboration for encouragement and feedback. This work was supported by the U.S. Department of Energy, Office of Science under contract DE-AC02-05CH11231.

A Rectangular pixels

The results presented thus far were based on the simulation of pixels with symmetric side lengths (i.e. square). However, there has been considerable investigation of the potential use of asymmetric pixels at the LHC, such as $25{\times}100\,\mu\text{m}^2$, which can trade off the position resolution in the longitudinal direction (z_0) for the increased resolution in the transverse direction (d_0), which is more important for flavor tagging. Importantly, when pixels are not square, the charge sharing will not be the same for the long and the short sides. While the complete calculation of charge sharing is complicated and sensor-specific, the capacitance (and thus the charge sharing) is approximately proportional to the side length of the pixel. For example, in the $25 \times 100\,\mu\text{m}^2$ case, the short sides will exhibit 4 times less charge sharing than the long sides.

Figure 6 illustrates how the position resolution changes with asymmetric pixels. In order to control for effects related to the actual amount of charge deposited due to the pixel size, all results are actually simulated with the $50 \times 50\,\mu\text{m}^2$ setup from earlier. However, the amount of sharing in the x and y directions is now different and is set proportional to the side length. If the sharing before was f_{share}, then the new sharing is $f'_{\text{share}} = 2f_{\text{share}}/(1 + \text{pixel asym.})$, which is chosen so that the total charge lost by the primary pixel is still $4f_{\text{share}}$. The pixel asymmetry is the ratio of the transverse to longitudinal pixel pitch.

The left plot of figure 6 shows how the relative resolution changes for different configurations as a function of the amount of charge sharing. A charge sharing value of 5% means that the primary pixel loses $4 \times 5\%$ of its charge to its neighbors, divided up in a way that is proportional to the shared side length. When the pitch is smaller, the optimal amount of charge sharing increases. In the $25 \times 100\,\mu\text{m}^2$ configuration, the optimal sharing for the long side is about 3% while there is

2019 JINST 14 P09028

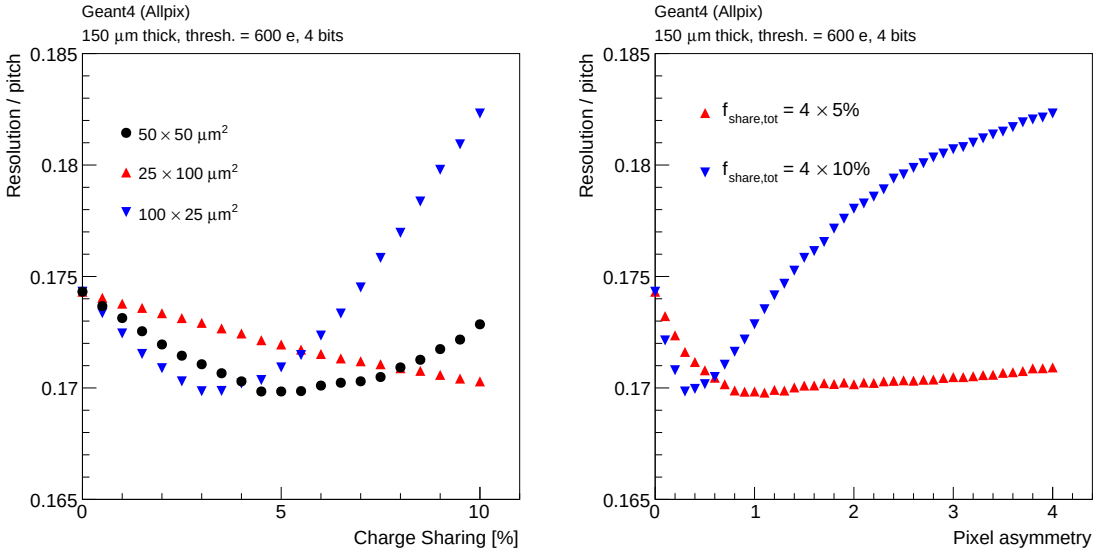

Figure 6. Left: the relative position resolution as a function of the amount of charge sharing for three different pixel configurations (the resolution always corresponds to the first dimension given in the legend). Right: for a fixed amount of total charge sharing (20% charge loss from the primary pixel), the position resolution is shown as a function of the asymmetry in the pixel pitches. A value of 0.25 corresponds to $25 \times 100\,\mu\text{m}^2$.

no optimal value for the short side (larger value than the 10% cutoff is desired). The right plot of figure 6 fixes the total charge sharing and varies the pixel asymmetry. For a total charge sharing of 5%, the down-triangles and circles from the left plot of figure 6 are nearly the same, which is consistent with the broad minimum in the right plot for the up-triangles. In contrast, there is a strong dependence on the pixel asymmetry in the sub-optimal case of 10% charge sharing.

B Noise sharing

The impact of noise on the position resolution is relatively small, in part because of the optimal use of charge information. However, one effect that was not considered in our previous analysis is the interplay between charge sharing and noise. The capacitive coupling that links pixels together shares noise as well as deposited charge. This brief section presents a study investigating the impact of this noise sharing.[8] Figure 7 shows the impact of ignoring noise sharing by showing the relative difference between the position resolution computed with and without noise sharing (but with charge sharing). For noise levels within the specification of the ATLAS and CMS pixel upgrades ($\lesssim 75\ e^-$ ENC [28]), the interplay between charge sharing and noise is small compared to the raw effect of charge sharing on resolution shown in figure 3. Consequently, such effects do not alter the conclusions drawn from the primary analysis of this work.

[8]For an analytic discussion for strip detectors using a simple linear interpolation for position estimation, see ref. [27].

2019 JINST 14 P09028

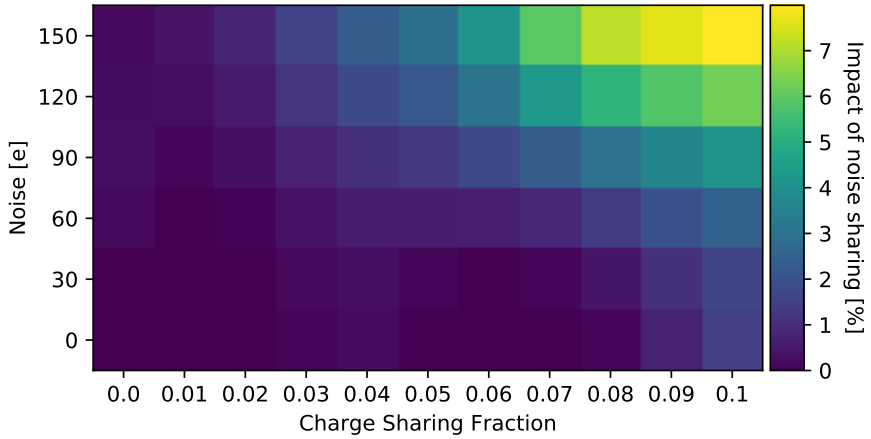

Figure 7. The relative change in the position resolution between two simulations: one incorporating both charge and noise sharing, and the other only charge sharing. In order to properly account for noise in neighboring pixels, entire pixel clusters were considered (an extension of the method presented in section 2.2) and analyzed with a simple neural network using standard tools [29–31]. This reduces to the method in the main body when ignoring such configurations.

References

[1] ATLAS IBL collaboration, *Production and Integration of the ATLAS Insertable B-Layer*, 2018 *JINST* **13** T05008 [arXiv:1803.00844].

[2] CMS collaboration, *Commissioning and Performance of the CMS Pixel Tracker with Cosmic Ray Muons*, 2010 *JINST* **5** T03007 [arXiv:0911.5434].

[3] L. Rossi, P. Fischer, T. Rohe and N. Wermes, *Pixel detectors: from fundamentals to applications*, Particle Acceleration and Detection, Springer, Berlin (2006).

[4] RD53 collaboration, *RD53A Integrated Circuit Specifications*, CERN-RD53-PUB-15-001.

[5] ATLAS collaboration, *Technical Design Report for the ATLAS Inner Tracker Pixel Detector*, CERN-LHCC-2017-021.

[6] CMS collaboration, *The Phase-2 Upgrade of the CMS Tracker*, CERN-LHCC-2017-009.

[7] ATLAS collaboration, *Pixel neighbour occupancy plots*, ITK-2016-003.

[8] L. Rossi, P. Fischer, T. Rohe, N. Wermes, *Pixel Detectors: From Fundamentals to Applications*, Springer-Verlag Berlin Heidelberg (2006).

[9] M. Garcia-Sciveres and T. Heim, *Self-Adjusting Threshold Mechanism for Pixel Detectors*, *Nucl. Instrum. Meth.* **A 867** (2017) 209 [arXiv:1701.01459].

[10] M.D. Rolo et al., *TOFPET ASIC for PET applications*, 2013 *JINST* **8** C02050.

[11] CMS collaboration, *Technical proposal for a mip timing detector in the CMS experiment phase 2 upgrade*, CERN-LHCC-2017-027.

[12] CMS-TOTEM collaboration, *CMS-TOTEM Precision Proton Spectrometer*, CERN-LHCC-2014-021.

[13] O. Merle et al., *Development of an Endcap DIRC for PANDA*, *Nucl. Instrum. Meth.* **A 766** (2014) 96.

[14] M. Da Rocha Rolo et al., *A custom readout electronics for the BESIII CGEM detector*, 2017 *JINST* **12** C07017 [arXiv:1706.02267].

2019 JINST 14 P09028

[15] K. Einsweiler, A. Joshi, R. Marchesini, F. Pengg and G. Zizka, *On the performance and limitations of a dual threshold discriminator pixel readout circuit for LHC*, *IEEE Trans. Nucl. Sci.* **46** (1999) 792.

[16] J. Cabello et al., *A dual threshold method to independently control spatial resolution and sensitivity in β imaging*, *IEEE Nucl. Sci. Symp. Conf. Rec.* (2008) 1.

[17] ALIBAVA collaboration, *A portable readout system for silicon microstrip sensors*, *Nucl. Instrum. Meth.* **A 623** (2010) 207.

[18] J. Idarraga and M. Benoit, *Generic Geant4 implementation for pixel detectors*, The AllPix Simulation Framework (2006) [twiki.cern.ch:AllPix].

[19] GEANT4 collaboration, *GEANT4: A Simulation toolkit*, *Nucl. Instrum. Meth.* **A 506** (2003) 250.

[20] Y. Chen et al., *Optimal use of Charge Information for the HL-LHC Pixel Detector Readout*, *Nucl. Instrum. Meth.* **A 902** (2018) 197 [arXiv:1710.02582].

[21] F. Wang, S. Dong, B. Nachman, M. Garcia-Sciveres and Q. Zeng, *The Impact of Incorporating Shell-corrections to Energy Loss in Silicon*, *Nucl. Instrum. Meth.* **A 899** (2018) 1 [arXiv:1711.05465].

[22] I. Kipnis et al., *A time-over-threshold machine: The readout integrated circuit for the BaBar silicon vertex tracker*, *IEEE Trans. Nucl. Sci.* **44** (1997) 289.

[23] F. Moscatelli et al., *Effects of Interface Donor Trap States on Isolation Properties of Detectors Operating at High-Luminosity LHC*, *IEEE Trans. Nucl. Sci.* **64** (2017) 2259.

[24] R. Dalal, *Simulation of Irradiated Detectors*, PoS(Vertex2014)030.

[25] DELPHI collaboration, *The DELPHI silicon strip microvertex detector with double sided readout*, *Nucl. Instrum. Meth.* **A 368** (1996) 314.

[26] F. Wang, B. Nachman and M. Garcia-Sciveres, *Ultimate position resolution of pixel clusters with binary readout for particle tracking*, *Nucl. Instrum. Meth.* **A 899** (2018) 10 [arXiv:1711.00590].

[27] G. Lutz, *Correlated Noise in Silicon Strip Detector Readout*, *Nucl. Instrum. Meth.* **A 309** (1991) 545.

[28] M. Garcia-Sciveres, *Production chip combined requirements for ATLAS and CMS*, CERN-RD53-PUB-18-002.

[29] F. Chollet et al., *Keras*, https://keras.io (2017).

[30] M. Abadi et al., *Tensorflow: A system for large-scale machine learning*, *OSDI* **16** (2016) 265.

[31] D.P. Kingma and J. Ba, *Adam: A Method for Stochastic Optimization*, arXiv:1412.6980.

2019 JINST 14 P09028